Dip pen nanolithography-deposited zinc oxide nanorods on a CMOS MEMS platform for ethanol sensing

S. Santra[a], A. De Luca[b], S. Bhaumik[a] , S. Z. Ali[c], F. Udrea[b,c], J. W. Gardner[c,d], S. K. Ray[a], P. K. Guha[e]*

[a]Department of Physics, Indian Institute of Technology, Kharagpur, India, 721302

[b]Engineering Department, University of Cambridge, Cambridge, CB3 0FA, UK

[c]Cambridge CMOS Sensors Ltd., Cambridge, CB4 0DL, UK

[d]School of Engineering, University of Warwick, Coventry, CV4 7AL, UK

[e]E & ECE Department, Indian Institute of Technology, Kharagpur, India, 721302

*Corresponding author E-mail: susmita.santra@phy.iitkgp.ernet.in

Abstract

This paper reports on the novel deposition of zinc oxide (ZnO) nanorods using dip pen nanolithographic (DPN) technique on SOI (silicon on insulator) CMOS MEMS (micro electro mechanical system) micro-hotplates (MHP) and their characaterisation as a low-cost, low-power ethanol sensor. The ZnO nanorods were synthesized hydrothermally and deposited on the MHP that comprises a tungsten micro-heater embedded in a dielectric membrane with gold interdigitated electrodes (IDEs) on top of an oxide passivation layer. The micro-heater and IDEs were used to heat up the sensing layer and measure its resistance, respectively. The sensor device is extremely power efficient because of the thin SOI membrane. The electro-thermal efficiency of the MHP was found to be 8.2°C/mW, which results in only 42.7 mW power at an operating temperature of 350°C. The CMOS MHP devices with ZnO nanorods were exposed to PPM levels of ethanol in humid air. The sensitivity achieved from the sensor was found to be 5.8%/ppm to 0.39%/ppm for the ethanol concentration range 25 – 1000 ppm. The ZnO nanorods showed optimum response at 350°C. The CMOS sensor was found to have a humidity dependence that needs consideration in real-world application. The sensors were also found to be selective towards ethanol when tested in presence of toluene and acetone. We believe that the integration of ZnO nanorods using DPN lithography with a CMOS MEMS substrate offers a low cost, low power, smart ethanol sensor that could be exploited in consumer electronics.

Keywords: Zinc oxide nanorods, MEMS, SOI CMOS, ethanol sensor, gas sensor, dip pen nanolithography

1. Introduction

Gas sensors have enjoyed a wide range of applications since the 1970s that is steadily growing. Nowadays, they are extensively used to detect hazardous (i.e. toxic and explosive) gases present in industrial areas, indoors, and coal mines. More recently they are being explored to monitor trace levels of volatile organic compounds (VOCs) in human breath, which contains biomarkers for specific diseases[1, 2]. However, commercially available gas sensors are still bulky, expensive and, with the exception of electrochemical, consume a large amount of power (~ 0.5 W). Hence, recent research on gas sensors has shifted towards the development of miniaturised, low power, inexpensive and easy to integrate devices. Such sensors can be achieved by advances on two fronts, (A) better sensing layers (e.g. polymer, carbon nano material or metal oxide) and (B) better substrates (e.g. sensors can be developed on ceramic, silicon, flexible polymer or a CMOS-MEMS platform).

Carbon nano material (Carbon nanotube, graphene) can sense gases close to room temperature, but their response is generally disappointing[3-6]. Metal oxides on the other hand are another class of material which shows large response but usually at elevated temperatures (e.g. 350^{o}C), so needs large power.

Ceramic and silicon substrate have been extensively used for sensor development. Flexible substrates[3, 4, 6] have recently been introduced to develop large area flexible sensors. However all these platforms require separate interface electronics that incurs additional costs making them commercially limited. In this respect, CMOS-MEMS[7-9] technology is very promising for a new generation of smart low-cost gas sensors; because the fabrication process is well established, devices are miniaturised (< 4 mm^2) and their performances are reliable and reproducible (because of batch fabrication). Such sensors can also have on-chip interface electronics, which results in a further system miniaturization and cost reduction. MEMS technology integration with CMOS is critical for achieving low power consumption of the

sensor device through micro-heater thermal isolation schemes[9, 10]. Resistive sensors have an advantage when compared to other classes of gas sensors (e.g. electrochemical and optical), because resistive sensors are easier to integrate with CMOS-MEMS platform.

Nano-materials have very high surface to volume ratio, thus providing a significant gas response even with a small amount of materials. Therefore nano-materials are well suited for miniaturised CMOS gas sensor devices. Commercially available solid state gas sensors are generally metal oxide based (e.g. tin oxide or tungsten oxide). Gas sensors using different metal oxide nano-materials are already reported in the literature[1, 11-15]. Among them, zinc oxide (ZnO) is one of the most reported sensing materials[11, 14-22]. Because its preparation method is simple, inexpensive, it has good thermal and chemical stability, high electron mobility and it responds to several gases or volatile organic compounds. Different nano-structure of ZnO including nanoparticles[17, 21], nanorod[17-20, 23], nanowire[14, 22], nanotube[16], thin film[24], thick film[25] are reported as gas sensing layers.

Nano-materials are prepared in several ways like chemical and physical methods (chemical vapour deposition methods, physical vapour deposition methods, sputtering and evaporation), mechanical exfoliation, chemical exfoliation etc. Deposition of nano-materials on CMOS-MEMS devices is a challenging task. Chemical routes are not suitable for CMOS sensors as some chemicals can have a detrimental effect on the integrity of the chip. Physical methods need either shadow or lithographic masking. Several methods have been reported to integrate nano-materials with CMOS devices, e.g. local growth technique[9, 26] to grow carbon nanotubes (CNTs), hydrothermal method to grow zinc oxide nanowires[14]. These reported materials grown directly on the sensor device, however seed layers were required which need to be sputter coated. Inkjet printing[27, 28] is a technique suitable for the deposition of nano-materials. However, making a stable ink which can be deposited to required precision and stability is under development.

Dip pen nano-lithography (DPN) is an extremely flexible deposition method, with possible wafer level scalability, which has proved to be suitable for nano-materials integration on membrane based CMOS devices. Additionally, DPN does not require a time-consuming development of the material to be deposited (as for ink-jet printing); a highly viscous slurry is acceptable for most applications.

Here in this work zinc oxide nanorods (NRs) were prepared using hydrothermal method. The ZnO nanorods were deposited on a predefined electrode area of CMOS sensor devices using DPN. Finally the devices were tested in presence of ethanol in humid air. The humidity dependence on ethanol sensing was experimentally investigated. A cross-sensitivity study to other VOCs was also performed.

2. Experimental

2.1 Zinc oxide nanorods preparation

Initially a ZnO nano-particle seed layer was prepared for zinc oxide nanorods growth. The seed layer was needed to support nucleation and subsequent growth. The seed layer was prepared by dissolving 0.5 g zinc-acetate in 100 ml of 2-propanol. Then the mixture was ultrasonicated for one hour to make a uniform solution. This solution was drop casted on a beaker preheated at 200°C. White ZnO nanoparticles were formed from the rapid evaporation of the solution. This seed layer was well dispersed in 400 ml of water by continuous ultrasonication for two hours. In this solution 20 mM zinc nitrate and hexametheline tetramine were added and vigorously stirred for 10 minutes. This solution was kept on a hotplate at 90°C for five hours to allow ZnO nanorods extrusion. The final solution was cleaned several times with deionised water and air dried, in order to remove any chemical residue present in NRs.

2.2 CMOS MEMS device fabrication

The gas sensors devices are based on a SOI (silicon on insulator) CMOS MEMS micro-hotplate (MHP) technology. The cross-sectional view and the optical micrograph of the device are shown in **Fig. 1(a)** and **(b)**. The silicon die is only 1 mm × 1 mm in size. The devices were designed in Tanner Tools LEdit 15.2, using 1.0 µm SOI CMOS process and fabricated at a commercial foundry. Micro-hotplates comprised a micro-heater and interdigitated electrodes (IDEs), suspended in a dielectric membrane. Tungsten was used as metal for the micro-heater, in place of Al or polysilicon, because of its superior electro-thermal properties that resulted in extended device lifetime at high operating temperatures. The membrane structure was created using deep reactive ion etching (DRIE) technique. The buried oxide was used as the etch stop with the total membrane thickness being *ca*. 5 µm. The micro-heater and membrane diameters were 250 and 650 µm, respectively, with a ratio chosen to optimise the chip size with respect to power consumption. The micro-heater design was also optimised in order to achieve highly temperature uniformity of the sensing material. The details of this study are reported in[10, 29]. A silicon nitride layer passivated the whole chip area with exception of the pads' areas to contact heater and IDEs. The gold electrodes and the gold interconnects to the pads were made by a post-CMOS process within the same foundry. Gold electrodes were found to have a good ohmic contact with the sensing materials, a long time stability and a smaller feature size in comparison to Al IDEs. The width of each electrode finger is 5 µm. The separation between the electrodes is 5 µm. As a consequence of the high thermal isolation offered by the thin dielectric membrane and the heat sink effect provided by the sensor package[10, 30], the temperature of the substrate area of the chip is close to room temperature. CMOS circuitry, for heater temperature control or sensing layer resistance readout, can thus be integrated on-chip.

The power versus temperature plot of the device is presented in **Fig. 2**. The heater can reliably reach temperatures of 600°C with 73 mW of power in 15 ms, with an electro-thermal efficiency of 8.2°C/mW, and cool down to ambient temperature in about 30 ms.

2.3 Dip Pen Nanolithography deposition

ZnO nanorods were integrated onto the CMOS microhotplates with a dip pen nanolithographic system (NLP2000 by NanoInk). Dip pen nanolithography[31] is a unique scanning-probe lithographic technique enabling the deposition of patterns of various materials with sub-micron resolution. To date, DPN has been investigated as a possible nanofabrication technology in four main areas: (i) direct-writing of bio-molecular micro arrays, (ii) creating tailored chemical surfaces for the investigation of biological recognition processes down to cellular level, (iii) generating chemical templates for orthogonal materials' assembly, (iv) low-cost and rapid sub-micron structures prototyping with both top-down and bottom-up approaches. All the previously mentioned application areas exploit the excellent DPN in-plane resolution for the delivery of materials in pico-litre quantities. In this work, we used DPN to functionalize fragile CMOS membrane based microhotplates, exploiting the DPN system off-plane resolution and the high mechanical compliance offered by the cantilever-type pens, in order to "gently" deposit ZnO nanorods (mixed with terpineol) slurry on a relatively wide area (> 250 μm diameter) at once. The slurry contains 95% of ZnO and 5% of terpineol in weight percent. In order to achieve such a wide deposition area a double cantilever pen was used. Each cantilever is approximately 50 μm wide and 150 μm long and they are 50μm apart from each other. By fully dipping the cantilevers and part of the pen in the material reservoir (not only the cantilever tip underneath the cantilevers' end as usually done in a DPN process for deposition of tiny amount of material) and by appropriately controlling the deposition time (the contact time between cantilever and substrate is in the

seconds range) it is possible to load and then deposit enough slurry to coat the whole IDEs area. The volume of the deposited slurry was ~ 10pL/deposition. The chemical optimization of the slurry for obtaining a highly uniform layer is under study.

2.4 Characterisation

Optical microscope picture was taken with Nikon L-UEPI fitted with Nikon DX1200F digital camera. The morphological and structural study of ZnO NRs were performed using field emission scanning electron microscope (FESEM, Zeiss Gemini-Sigma), transmission electron microscopy (TEM, FEI – Tecnai G2 20S – Twin operated at 200 kV), X-ray diffraction (Philips X-Pert MRD with Cu Kα radiation). Electrical measurements were performed using a commercial precision instrument (Keithley 2401).

2.5 Automated gas testing station

The gas sensing measurements were performed at the Microsensors and Bioelectronics Laboratory, Warwick University using fully-automated custom rig. The CMOS die were mounted and ultrasonically wire bonded onto gold TO5 packages, in order to be connected to a custom made printed circuit board and housed inside the sensor chamber. Micro-heater and sensing material's resistance were respectively driven and measured *via* a LabView software. Control of the different valves and digital mass flow controllers of the gas system was also performed automatically through a Labview VI.

3. Results and Discussion

3.1 Morphology and structure

An optical microscope image of the DPN deposited ZnO nanorods on MHP is shown in **Fig. 3(a)**. A typical SEM image of the MHP with ZnO nanorods is shown in **Fig. 3(b)**. From these micrographs, it can be clearly seen that the nanorods are deposited mainly over the micro-heater region, without creating a thermal bridge from the hot-area to the substrate -

thus avoiding undesired extra power dissipation. In our previous reports[9, 14] vertically aligned ZnO nanowires[12] and carbon nanotubes[7,] were grown directly on the MHP. Here the nanorods (single or bundles) are horizontally bridging electrodes, resulting in a better lateral heat transfer, making it more important to avoid growing the nanorods in the membrane area between the heater and substrate. A magnified view of the nanorods is presented in the inset of **Fig. 3(b)**. The hexagonal structure of ZnO nanorods can be clearly noticed. Nanorods are 100 nm – 300 nm in diameter and more than 2 μm long. Transmission electron microscopy (TEM) image of ZnO as seen in **Fig. 3(c)** clearly signifies the rod like nano-structure. The X-ray diffraction (XRD) measurement, shown in **Fig. 3(d)**, has been performed to have a detailed insight of the structure of ZnO nanorod, which is shown to be polycrystalline and correspond to wurtzite structure.

3.2 Electrical Characterisation

The current voltage characteristics ($I - V$) were measured at different operating temperatures and are shown in **Fig. 4(a)**. A contact between a metal and semiconductor can be either Ohmic or Schottky in nature, depending upon the difference in the work function of the metal and electron affinity of semiconductor. When the work function is equal or lower than the electron affinity then the contact is ohmic. In our case the work function of Au (5.1 eV) is larger than the electron affinity (4.2 eV) of zinc oxide. Consequently, at ambient temperatures the contact is non-linear. But as we increase the temperature then the $I - V$ slope increases up to 350°C and becomes more linear (i.e. Ohmic). Thus the contact resistance is lower and can be ignored at higher temperature while performing the gas sensing measurements.

3.3 Gas response

In this work, the sensor response (S) is defined by the ratio R_a/R_g where R_a and R_g are the sensor electrical resistance in air and ethanol, respectively. Initially the ZnO sensor was tested in the presence of 1000 ppm ethanol in order to obtain the optimum working

temperature of the sensor, as shown in **Fig. 4(b)**. The sensor response increases with temperature and maximum response is found at 350°C. The response decreases above this temperature. Initially the reaction of gases with chemisorbed oxygen sites increases with increase in temperature. Above 350°C, the desorption rate is higher than the adsorption, so the response decreases with the further increase in temperature. Therefore, all the measurements have been performed at a temperature of 350°C. The DC power consumption required to operate at this temperature is 42.7 mW.

The time-dependent response to ethanol pulses at 10% relative humidity (RH) is shown in **Fig. 5(a)**. The peak gas concentration increases from 25 to 1000 ppm. The response is found to increase with increasing concentration as expected. The responses (R_a/R_g) at 25 and 1000 ppm are calculated to be 1.45 and 3.9, respectively. Sensitivity in percentage (defined as response/concentration) varies from 5.8%/ppm – 0.39%/ppm for the concentration range from 25 – 1000 ppm.

The response time is defined as the time taken by the sensor to reach 90% of the full response, whereas recovery time is the time required to reach the 10% of the sensor baseline resistance. Response and recovery times at different concentrations of ethanol are presented in **Fig. 5(b)**. It is observed that with increase in gas concentrations, the response time decreases whereas the recovery time increases. Response time ranged from 150 – 8 sec and recovery time 100 – 560 sec when the concentration is varied from 25 – 1000 ppm. The performance of DPN deposited ZnO nanorods is much better than our earlier report[14], e.g. the sensitivity is much higher (145% higher – in present work the sensitivity at 750 ppm is 0.49%/ppm as compared to 0.2%/ppm at 809 ppm of ethanol in earlier work). The response and recovery time is also much faster (in present work $t_{response}$ is only 9 sec and $t_{recovery}$ is 480 sec at 750 ppm whereas $t_{response}$ is 200 sec and $t_{recovery}$ is more than 10 min at 809 ppm in earlier work). In the present work we have detected ethanol concentration as low as 25 ppm

(the lowest concentration we could measure in our previous work was 809 ppm).These improved results can be attributed to the fact that ethanol molecules can react with the chemisorbed oxygen species at the surface of ZnO nanorod immediately. This is because nanorods are horizontally aligned on the electrodes instead of vertically standing, thus offering a wider surface for chemical interaction. Also, as the nanorods are horizontally aligned on the IDEs, so we believe heat transfer will be better than the rooted growth vertical nanorods. So the temperature of the film will be much more uniform than the rooted growth. As a result the response and recovery time will be better in this case. The obtained results (response, recovery and response time towards ethanol) are better than or comparable to the reported results available in literature[14, 23, 32-34]. Some reports are also available which are better than our results[16, 18, 20, 21]. It may be due to the different morphology and size of the nanostructures. The measurements were performed in dry air for some reports which provides better response than humid air measurements. However, most of the reported results are on non-CMOS platform which are not ideal for batch fabrication and commercialisation.

The response of semiconductor metal oxide gas sensor is empirically represented by the following power law:

$$S = 1 + A_g P_g^{\beta} = 1 + A_g C_g^{\beta} \qquad (1)$$

where A_g is the prefactor which depends on sensing materials, operating temperature and the type of gas interacting with the sensor. P_g is the partial pressure of gas which is directly proportional to concentration (C_g) of gas and β is the exponent factor. The ideal value of β is either 0.5 or 1 depending on the charged state of surface oxygen species and the stoichiometry of the elementary reactions on the surface. The value of β was calculated from the interaction between chemisorbed surface oxygen species and the reducing gases like ethanol. It was reported[35] that β is 1 or 0.5 when the surface oxygen species are O^- and O^{2-} state, respectively. In **Fig. 6** the experimentally measured response versus concentration is

plotted. A power law has been fitted through the experimental points according to equation (1). The value of β is 0.438±0.022, which is slightly lower than the ideal value (0.5). This could be due to the agglomeration of nano-materials or some area is less sensitive to ethanol[36]. The exponent β is nearer to 0.5 suggesting that the chemisorbed oxygen species are in O^{2-} state.

Zinc oxide sensors are known to be sensitive towards various organic vapours. Hence some selectivity measurements have also been performed and presented in **Fig. 7**. These sensors were tested in presence of 1000 ppm of ethanol, acetone and toluene. It is found that responses of acetone and toluene are 1.29 and 2.2, respectively. The response is 3 and 1.77 times lower than ethanol. Hence the ZnO sensors are selective towards ethanol. This observation is also in agreement with other reported result on ethanol sensor[21].

3.4 Sensing mechanism

The scheme for sensing mechanism of ZnO NR is presented in **Fig. 8**. When the semiconductor metal oxides are exposed to air, the oxygen molecules are adsorbed on the surface of the materials. At room temperature the oxygen molecules are physisorbed. As the temperature is increased, oxygen molecules are dissociated to atomic oxygen. Different oxygen species (O_2^-, O^-, O^{2-}) are created depending on the working temperature[23].

$$O_2(g) \rightarrow O_2(ads) \quad (2)$$

$$O_2(ads) + e^- \rightarrow O_2^-(ads) \quad T < 100°C \quad (3)$$

$$O_2^-(ads) + e^- \rightarrow 2O^-(ads) \quad 100°C \leq T \leq 300°C \quad (4)$$

$$O^-(ads) + e^- \rightarrow O^{2-}(ads) \quad T > 300°C \quad (5)$$

These oxygen species will take the electrons from the conduction band of the ZnO and chemisorbed on the surface. This creates an electron depletion layer on the surface of the material which increases the resistance of the sensing layer as shown in **Fig. 8 (a)**.

Ethanol interaction with metal oxide is complicated. Depending on the acid, base property of metal oxide ethanol will be decomposed to an intermediate state either to ethylene (dehydration) or acetaldehyde (dehydrogenation)[37, 38]. As ZnO is a basic oxide, ethanol will be converted to acetaldehyde by the following equation.

$$CH_3CH_2OH \rightarrow CH_3COH + H_2 \quad (6)$$

Acetaldehyde will be further oxidised by interacting with the chemisorbed oxygen species. As our working temperature is 350°C, O^{2-} species will mainly interact with ethanol by the following equation

$$CH_3CHO + 5O^{2-}(ads) \rightarrow 2CO_2(ads) + 2H_2O(vap) + 10e^- \quad (7)$$

It can be seen from the above equation that the electrons will be freed due to the reaction with ethanol and returned back to the conduction band of nanorods. Hence, the resistance of the ZnO nanorods will decrease in presence of ethanol as presented in **Fig. 8 (b)**.

3.5 Humidity effect on ethanol sensing

The ZnO sensor was also tested in presence of ethanol at dry air, 10% RH, 40% RH to see the humidity effect on sensing as shown in **Fig. 9**. In this case concentrations were varied from 100 ppm – 1000 ppm. At dry air, response varied from 2.9 – 6.1 as the concentrations were changing from 100 ppm – 1000 ppm. The corresponding values for 10% and 40% RH are 2 – 3.7 and 1.7 – 2.8, respectively. At 1000 ppm the response decreased by 1.67 and 2.17 times for 10% and 40% RH, respectively. Hence humidity plays a crucial role in sensing even at this high temperature.

When 10% RH was introduced inside the chamber, the conductivity of the ZnO nanorods increased very sharply as shown in inset of **Fig. 9** (red circular area). This fast change in resistance is due to the non-dissociative adsorption of water molecules as shown by the following equation[39]

$$H_2O(gas) \rightarrow H_2O(ads) \rightarrow H_2O^+(ads) + e^- \quad (8)$$

According to the above equation water molecules donate the electron to the conduction band of ZnO which is responsible for the fast change in resistance with the introduction of humidity. Illyaskutty et al.[39] also reported the similar conductivity change results in presence of humidity of molybdenum oxide. It was also observed that after the sharp decrease, the resistance increases slowly. This can be due to another second slow reaction started along with the process presented in equation (8). In the slow reaction, adsorbed water molecules broke into hydrogen and hydroxyl group[39] due to the high working temperature.

$$H_2O(ads) \rightarrow OH(ads) + H(ads) \quad (9)$$

This hydroxyl group interacts with Zn and hydrogen reacts with lattice oxygen by the following equation[14, 39].

$$H_2O(ads) + Zn_{lat} + O_{lat} \rightarrow (HO - Zn_{lat}) + (O_{lat}\,H)^+ + V_o^{2+} + e^- \quad (10)$$

where V_o^{2+} is the oxygen vacancy. After initial increase of conductivity, the reactions presented in (8) and (10) progress simultaneously, thus slowly decreasing the conductivity of the nanorods. In this condition when ethanol is introduced the response was found to decrease, in comparison to dry air condition. The reasons for such behaviour are two fold[40, 41]. Firstly, some active sites are blocked by hydroxyl groups. Secondly, there is a competition between water molecules and ethanol to react with adsorbed species which eventually decrease response towards ethanol. Similar observations have also been demonstrated for other metal oxides towards ethanol sensing[39, 41].

4. Conclusions

Zinc oxide nanorods were successfully integrated with SOI CMOS MEMS platform using dip pen nanolithography. The zinc oxide nanorods were prepared hydrothermally. CMOS MEMS gas sensors are found to be power efficient and on-chip electronic circuit integration is possible. The ethanol sensing performance was investigated in the temperature range 250°C –

450°C and the optimum operating temperature was found to be at 350°C. Ethanol sensitivity was found to be 5.8 %/ppm – 0.39 %/ppm for the concentration range 25 ppm – 1000 ppm. The response and recovery times are found to be 9 s and 480 s at 750 ppm of ethanol, respectively. The CMOS sensors were tested in presence of ethanol, toluene and acetone in humid air. The sensor is found to be selective towards ethanol. The response was found to decrease in humid ambience as compared to dry air environment. The study indicates that DPN deposited ZnO nanorods on CMOS substrate may open up a scalable, batch produced approach to develop power efficient, low cost smart ethanol sensor.

Acknowledgements

S. Santra acknowledges Department of Science and Technology (DST) for Ramanujan Fellowship (project no. SR/S2/RJN-104/2011). This work was (partly) supported through the EU FP7 projects SOI-HITS (288481), GRAPHOL (2852754) and MSP (611887).

References

1. J. Shin, S.-J. Choi, I. Lee, D.-Y. Youn, C. O. Park, J.-H. Lee, H. L. Tuller and I.-D. Kim, *Advanced Functional Materials*, 2013, **23**, 2357-2367.
2. G. Peng, M. Hakim, Y. Y. Broza, S. Billan, R. Abdah-Bortnyak, A. Kuten, U. Tisch and H. Haick, *British Journal of Cancer*, 2010, **103**, 542-551.
3. S. Ammu, V. Dua, S. R. Agnihotra, S. P. Surwade, A. Phulgirkar, S. Patel and S. K. Manohar, *Journal of the American Chemical Society*, 2012, **134**, 4553-4556.
4. K. A. Mirica, J. G. Weis, J. M. Schnorr, B. Esser and T. M. Swager, *Angewandte Chemie-International Edition*, 2012, **51**, 10740-10745.
5. F. Schedin, A. K. Geim, S. V. Morozov, E. W. Hill, P. Blake, M. I. Katsnelson and K. S. Novoselov, *Nature Materials*, 2007, **6**, 652-655.

6. J. W. Han, B. Kim, J. Li and M. Meyyappan, *Journal of Physical Chemistry C*, 2012, **116**, 22094-22097.

7. C. Hagleitner, A. Hierlemann, D. Lange, A. Kummer, N. Kerness, O. Brand and H. Baltes, *Nature*, 2001, **414**, 293-296.

8. J. S. Suehle, R. E. Cavicchi, M. Gaitan and S. Semancik, *Ieee Electron Device Letters*, 1993, **14**, 118-120.

9. S. Santra, S. Z. Ali, P. K. Guha, G. F. Zhong, J. Robertson, J. A. Covington, W. I. Milne, J. W. Gardner and F. Udrea, *Nanotechnology*, 2010, **21**, 7.

10. S. Z. Ali, F. Udrea, W. I. Milne and J. W. Gardner, *Journal of Microelectromechanical Systems*, 2008, **17**, 1408-1417.

11. Y. Qiu and S. Yang, *Advanced Functional Materials*, 2007, **17**, 1345-1352.

12. C. Wang, D. Cai, B. Liu, H. Li, D. Wang, Y. Liu, L. Wang, Y. Wang, Q. Li and T. Wang, *Journal of Materials Chemistry A*, 2014, **2**, 10623-10628.

13. S. Vallejos, P. Umek, T. Stoycheva, F. Annanouch, E. Llobet, X. Correig, P. De Marco, C. Bittencourt and C. Blackman, *Advanced Functional Materials*, 2013, **23**, 1313-1322.

14. S. Santra, P. K. Guha, S. Z. Ali, P. Hiralal, H. E. Unalan, J. A. Covington, G. A. J. Amaratunga, W. I. Milne, J. W. Gardner and F. Udrea, *Sensors and Actuators B-Chemical*, 2010, **146**, 559-565.

15. N. Gogurla, A. K. Sinha, S. Santra, S. Manna and S. K. Ray, *Scientific Reports*, 2014, **4**.

16. Q. Yu, C. Yu, J. Wang, F. Guo, S. Gao, S. Jiao, H. Li, X. Zhang, X. Wang, H. Gao, H. Yang and L. Zhao, *Rsc Advances*, 2013, **3**, 16619-16625.

17. R. C. Singh, O. Singh, M. P. Singh and P. S. Chandi, *Sensors and Actuators B-Chemical*, 2008, **135**, 352-357.

18. S. Tian, F. Yang, D. Zeng and C. Xie, *Journal of Physical Chemistry C*, 2012, **116**, 10586-10591.

19. L. Wang, Y. Kang, X. Liu, S. Zhang, W. Huang and S. Wang, *Sensors and Actuators B-Chemical*, 2012, **162**, 237-243.

20. Z. Wen, L. Zhu, Z. Zhang and Z. Ye, *Sensors and Actuators B-Chemical*, 2015, **208**, 112-121.

21. S. Wei, S. Wang, Y. Zhang and M. Zhou, *Sensors and Actuators B-Chemical*, 2014, **192**, 480-487.

22. T.-J. Hsueh, C.-L. Hsu, S.-J. Chang and I. C. Chen, *Sensors and Actuators B-Chemical*, 2007, **126**, 473-477.

23. M. Z. Ahmad, A. Z. Sadek, K. Latham, J. Kita, R. Moos and W. Wlodarski, *Sensors and Actuators B-Chemical*, 2013, **187**, 295-300.

24. G. K. Mani and J. B. B. Rayappan, *Sensors and Actuators B-Chemical*, 2013, **183**, 459-466.

25. M. S. Wagh, G. H. Jain, D. R. Patil, S. A. Patil and L. A. Patil, *Sensors and Actuators B-Chemical*, 2006, **115**, 128-133.

26. M. S. Haque, K. B. K. Teo, N. L. Rupensinghe, S. Z. Ali, I. Haneef, S. Maeng, J. Park, F. Udrea and W. I. Milne, *Nanotechnology*, 2008, **19**.

27. S. M. C. Vieira, P. Beecher, I. Haneef, F. Udrea, W. I. Milne, M. A. G. Namboothiry, D. L. Carroll, J. Park and S. Maeng, *Applied Physics Letters*, 2007, **91**.

28. F. Torrisi, T. Hasan, W. Wu, Z. Sun, A. Lombardo, T. S. Kulmala, G.-W. Hsieh, S. Jung, F. Bonaccorso, P. J. Paul, D. Chu and A. C. Ferrari, *ACS Nano*, 2012, **6**, 2992-3006.

29. P. K. Guha, S. Z. Ali, C. C. C. Lee, F. Udrea, W. I. Milne, T. Iwaki, J. A. Covington and J. W. Gardner, *Sensors and Actuators B-Chemical*, 2007, **127**, 260-266.

30. S. Santra, P. K. Guha, S. Z. Ali, I. Haneef and F. Udrea, *IEEE Sensors Journal*, 2008, **10**, 997-1003.

31. D. S. Ginger, H. Zhang and C. A. Mirkin, *Angewandte Chemie-International Edition*, 2004, **43**, 30-45.

32. H. J. Pandya, S. Chandra and A. L. Vyas, *Sensors and Actuators B-Chemical*, 2012, **161**, 923-928.

33. N. Van Hicu and N. D. Chien, *Physica B-Condensed Matter*, 2008, **403**, 50-56.

34. W.-Y. Wu, J.-M. Ting and P.-J. Huang, *Nanoscale Research Letters*, 2009, **4**, 513-517.

35. S. Choopun, N. Hongsith, P. Mangkorntong and N. Mangkorntong, *Physica E-Low-Dimensional Systems & Nanostructures*, 2007, **39**, 53-56.

36. R. W. J. Scott, S. M. Yang, G. Chabanis, N. Coombs, D. E. Williams and G. A. Ozin, *Advanced Materials*, 2001, **13**, 1468-+.

37. T. Rakshit, S. Santra, I. Manna, S. K. Ray, *RSC Advances*, 2014, **4**, 36749-36756.

38. S. Shi, Y. Liu, Y. Chen, J. Zhang, Y. Wang and T. Wang, *Sens. Actuators, B*, 2009, **140**, 426–431

39. N. Illyaskutty, H. Kohler, T. Trautmann, M. Schwotzer and V. P. M. Pillai, *Sensors and Actuators B-Chemical*, 2013, **187**, 611-621.

40. P. R. S. Medeiros, J. G. Eon and L. G. Appel, *Catalysis Letters*, 2000, **69**, 79-82.

41. F. Pourfayaz, A. Khodadadi, Y. Mortazavi and S. S. Mohajerzadeh, *Sensors and Actuators B: Chemical*, 2005, **108**, 172-176.

Figure Captions

Fig. 1 (a) Cross sectional view of the CMOS MEMS micro-hotplate technology (b) Optical micrograph of fabricated device (1mm by 1mm).

Fig. 2 Power versus temperature plot of tungsten micro-heater.

Fig. 3 (a) Optical microscope picture of micro-hotplate with ZnO nanorods, (b) Typical SEM image of ZnO NRs on MHP, a magnified view of nanorods is shown in the inset (c) TEM image of ZnO nanorods, (d) XRD spectrum of ZnO nanorods.

Fig. 4 (a) $I - V$ characteristic ZnO NRs on gold IDEs at different temperatures, (b) Sensor response as a function of temperature for 1000 ppm of ethanol in 10% RH air.

Fig. 5 (a) Dynamic response of ZnO NRs in presence of ethanol at 350°C, (b) Response and recovery time against ethanol concentration plot at 350°C.

Fig. 6 Response of ZnO nanorods sensor as a function of concentration plot. Solid line represents the power law fitted through the experimental points.

Fig. 7 Selectivity measurements of ZnO NRs for 1000 ppm concentration.

Fig. 8 (a) ZnO NR in presence of air, (b) ethanol and their corresponding band diagrams.

Fig. 9 Ethanol sensing measurements in presence of dry, 10% RH and 40% RH air.

TOC caption: Zinc oxide nanorods integration with CMOS MEMS substrate using dip pen nanolithography for low cost, low power ethanol sensor development.

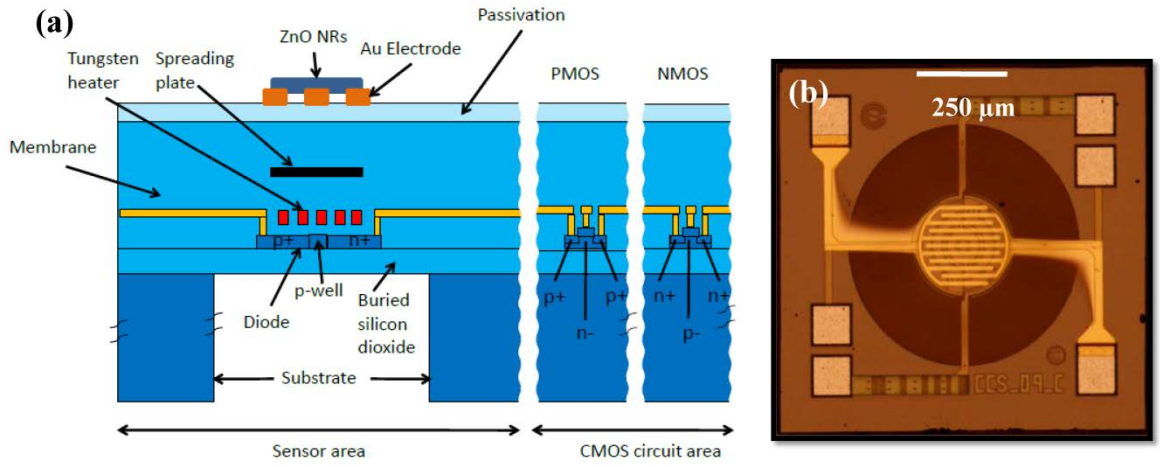

Fig. 1 (a) Cross sectional view of the CMOS MEMS micro-hotplate technology (b) Optical micrograph of fabricated device (1mm by 1mm).

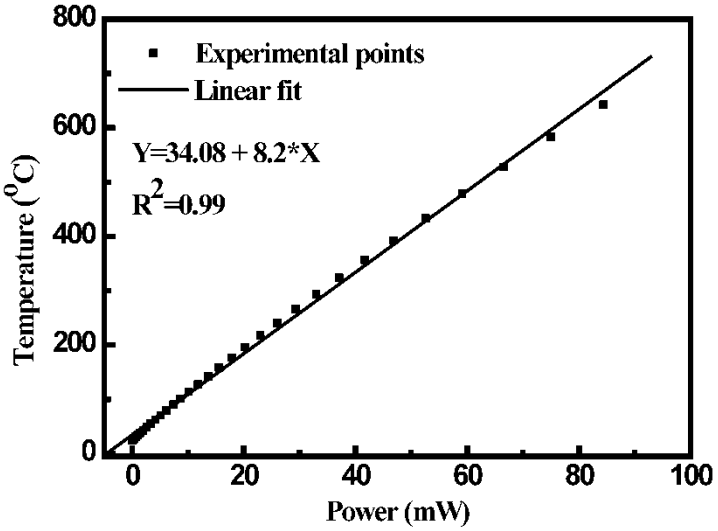

Fig. 2 Power versus temperature plot of tungsten micro-heater.

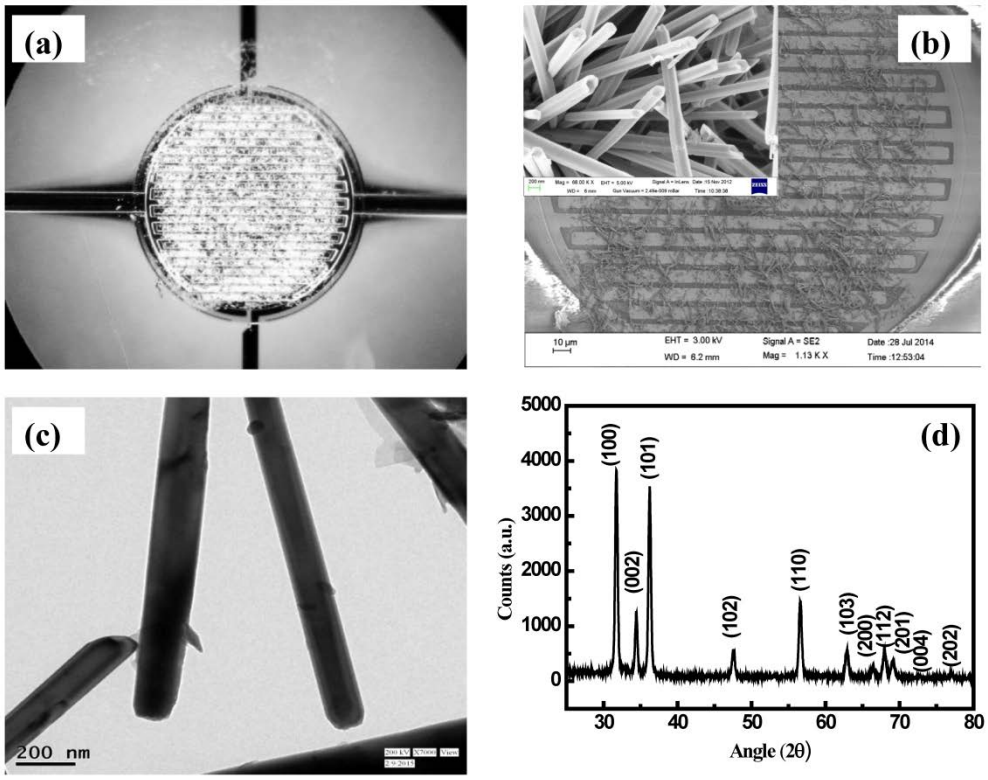

Fig. 3 (a) Optical microscope picture of micro-hotplate with ZnO nanorods, (b) Typical SEM image of ZnO NRs on MHP, a magnified view of nanorods is shown in the inset (c) TEM image of ZnO nanorods, (d) XRD spectrum of ZnO nanorods.

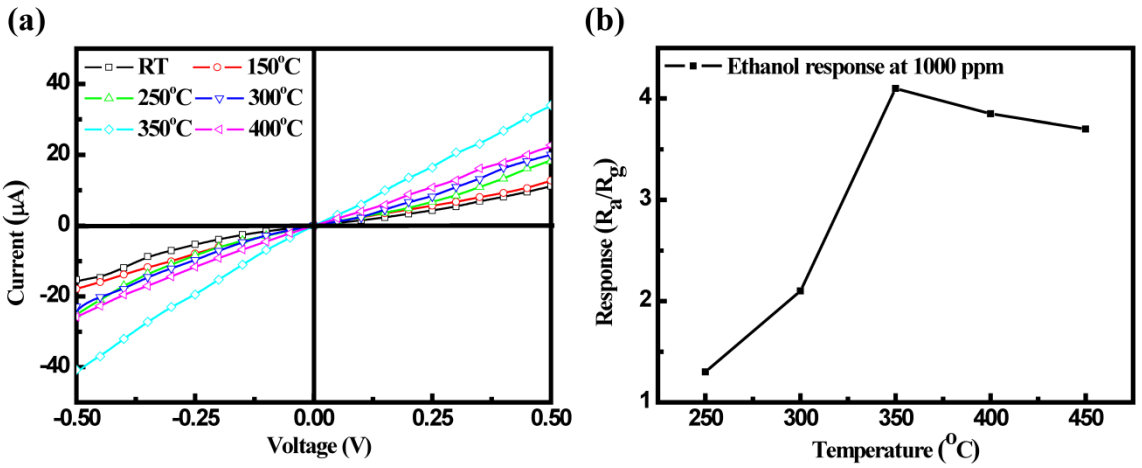

Fig. 4 (a) *I* – *V* characteristic ZnO NRs on gold IDEs at different temperatures, (b) Sensor response as a function of temperature for 1000 ppm of ethanol in 10% RH air.

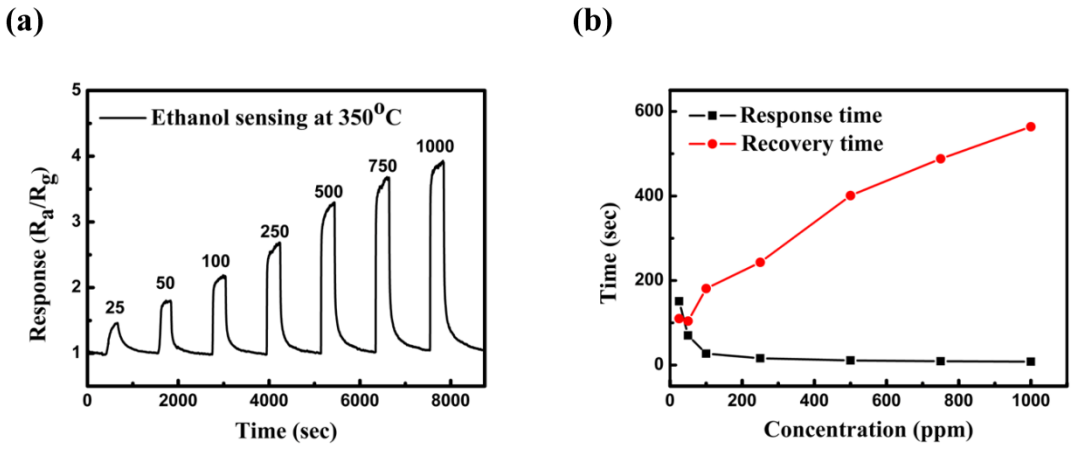

Fig. 5 (a) Dynamic response of ZnO NRs in presence of ethanol at 350°C, (b) Response and recovery time against ethanol concentration plot at 350°C.

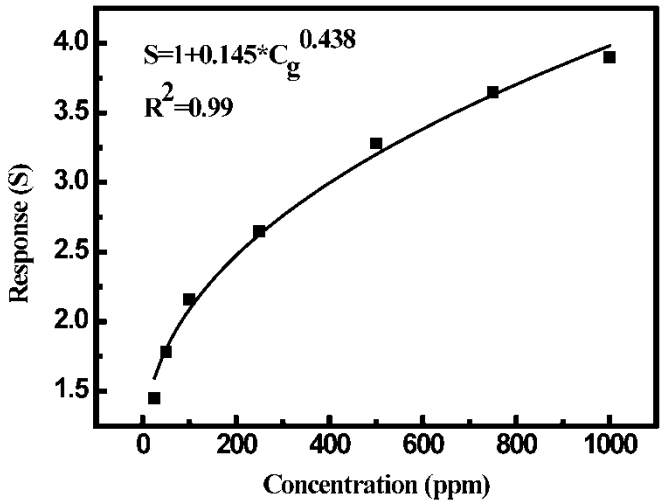

Fig. 6 Response of ZnO nanorods sensor as a function of concentration plot. Solid line represents the power law fitted through the experimental points.

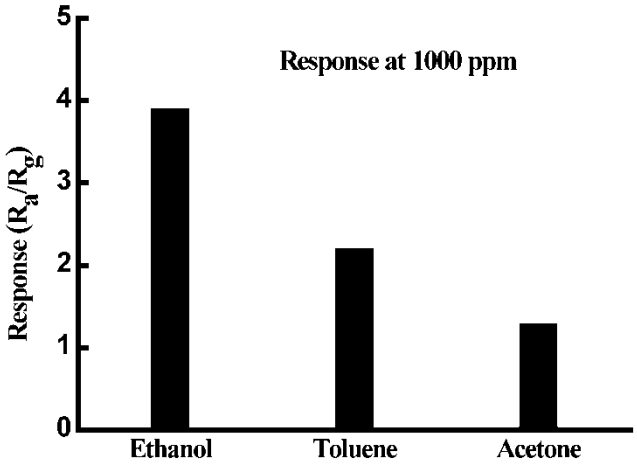

Fig. 7 Selectivity measurements of ZnO NRs for 1000 ppm concentration.

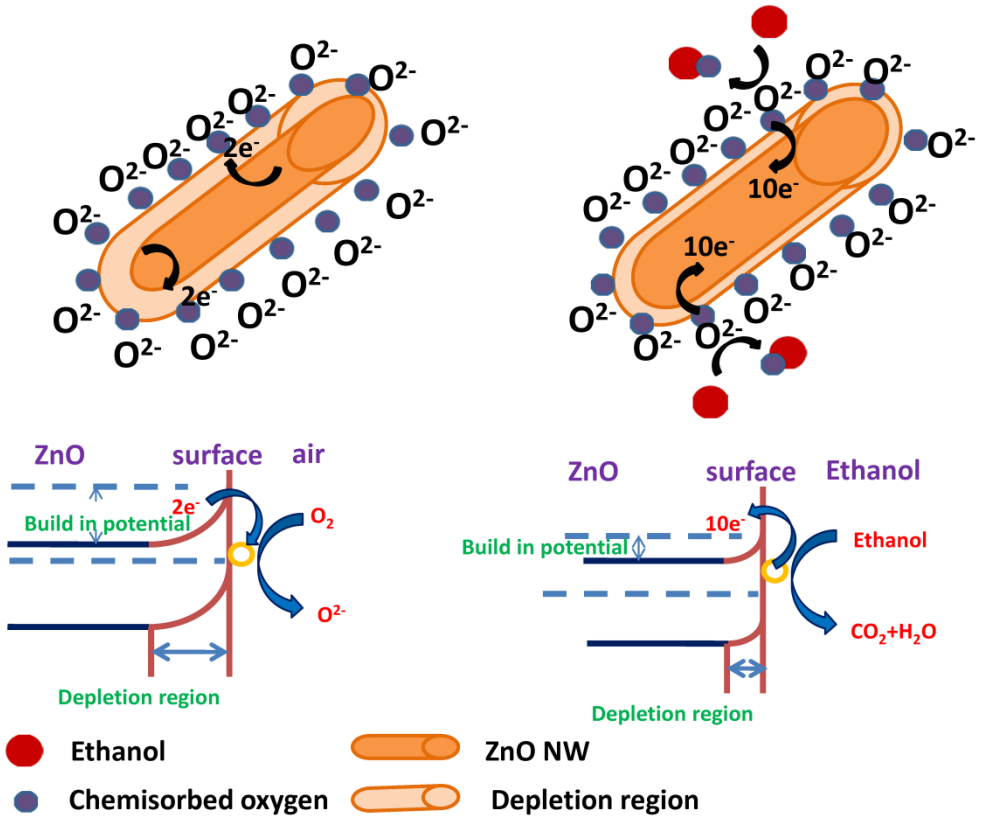

Fig. 8 (a) ZnO NR in presence of air, (b) ethanol and their corresponding band diagrams.

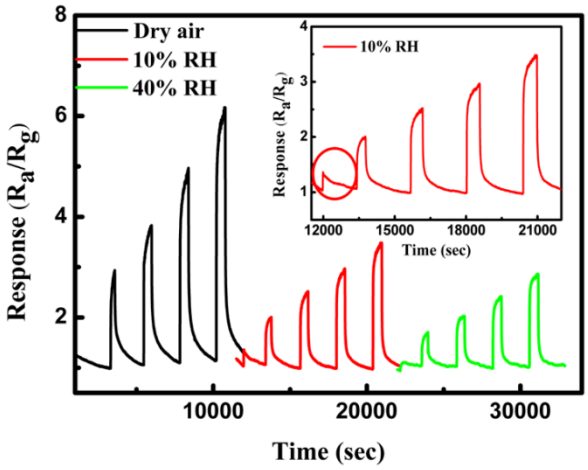

Fig. 9 Ethanol sensing measurements in presence of dry, 10% RH and 40% RH air.

Table of content

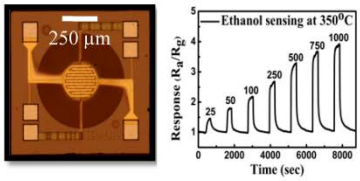

Zinc oxide nanorods integration with CMOS MEMS substrate using dip pen nanolithography for low cost, low power ethanol sensor development.